

Rolling Waves with Non-Paraxial Phonon Spins

Peng Zhang,¹ Christian Kern,² Sijie Sun,³ David A. Weitz,³ and Pai Wang¹

¹Department of Mechanical Engineering, University of Utah, Salt Lake City, UT 84112, USA

²Department of Mathematics, University of Utah, Salt Lake City, UT 84112, USA

³Harvard John A. Paulson School of Engineering and Applied Science, Harvard University, Cambridge, MA 02138, USA

(Dated: Submitted for review on July 02, 2020)

We demonstrate a new class of elastic waves in the bulk: When longitudinal and transverse components propagate at the same speed, rolling waves with a spin that is not parallel to the wave vector can emerge. First, we give a general definition of spin for traveling waves. Then, since rolling waves cannot exist in isotropic solids, we derive conditions for anisotropic media and proceed to design architected materials capable of hosting rolling waves. Numerically, we show spin manipulations by reflection. Structures reported in this work can be fabricated using available techniques, opening new possibilities for spin technologies in acoustics, mechanics and phononics.

The intrinsic spin angular momentum is an important property not only in quantum mechanical descriptions of fundamental particles but also in polarization representations of general wave mechanics [1–3]. For electromagnetic and elastic waves, the transversely circular polarization has a direct correspondence to the spin-1 photons [4, 5] and phonons [6–10], respectively. This duality between the classical and quantum worlds has inspired a number of recent studies in optics [11–14], gravitational waves [15], acoustics [16–20] and solid mechanics [21–23]. Many intriguing features have been demonstrated, including spin-orbit coupling [24, 25], spin-momentum locking [26] and topological edge states analogous to the quantum spin Hall effect [27–30].

Focusing on elastic waves in solids, we note that there is naturally a *traveling* longitudinal component (Fig. 1(a)), which can co-propagate with shear waves (Fig. 1(b)). This is in stark contrast with electromagnetic waves, for which the longitudinal component can only exist either due to localized interference [4, 5], with field

couplings [11–13], or as evanescent waves [14]. Consequently, in addition to the usual paraxial spin carried by shear waves (Figs. 1(c) and 1(d)), elastic waves may also carry spins corresponding to the displacement trajectory rolling forward (Fig. 1(e)) or rolling backward (Fig. 1(f)). Such special cases of non-paraxial spins are also referred to as “transverse spins” [31, 32], as the spin vector here is perpendicular to the wave vector. Importantly, recent research has proposed hybrid spins of two elastic waves using interference patterns, i.e., a localized superposition of waves in different directions [1]. Differently, here we report new results on *traveling* rolling waves with *propagating* non-paraxial spins, which are defined as follows: We consider the displacement field of a general plane wave $\mathbf{u} = \tilde{\mathbf{u}} \exp(i\mathbf{k} \cdot \mathbf{r} - i\omega t)$ with

$$\tilde{\mathbf{u}} = \frac{A}{\sqrt{|m|^2 + |n|^2 + |l|^2}} \begin{pmatrix} m \\ n \\ l \end{pmatrix}, \quad (1)$$

where A denotes the amplitude. Importantly, here m , n and l are complex-valued, so that they contain the information about not only relative amplitudes but also *relative phase differences* among the displacement components. The spin angular momentum density, as a real-valued vector, can be calculated as [1, 2, 33]:

$$\mathbf{s} = \frac{\rho\omega}{2} \langle \tilde{\mathbf{u}} | \hat{\mathbf{S}} | \tilde{\mathbf{u}} \rangle = \frac{\rho\omega}{2} \text{Im}[\tilde{\mathbf{u}}^* \times \tilde{\mathbf{u}}], \quad (2)$$

where $(\cdot)^*$ denotes complex conjugation, and the spin-1 operator is defined as

$$\hat{\mathbf{S}} = \left[\begin{pmatrix} 0 & 0 & 0 \\ 0 & 0 & -i \\ 0 & i & 0 \end{pmatrix}, \begin{pmatrix} 0 & 0 & i \\ 0 & 0 & 0 \\ -i & 0 & 0 \end{pmatrix}, \begin{pmatrix} 0 & -i & 0 \\ i & 0 & 0 \\ 0 & 0 & 0 \end{pmatrix} \right]. \quad (3)$$

Hence, the spin density for a general traveling wave is

$$\mathbf{s} = \frac{\rho\omega A^2}{|m|^2 + |n|^2 + |l|^2} \text{Im} \begin{pmatrix} n^* l \\ l^* m \\ m^* n \end{pmatrix}. \quad (4)$$

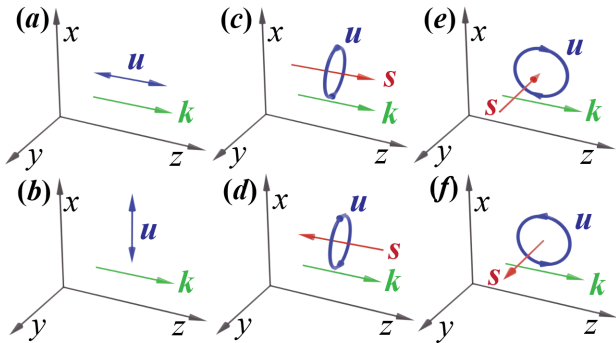


FIG. 1. Spin categories of bulk elastic waves: (a) linear longitudinal $(m, n, l) = (0, 0, 1)$ and (b) linear transverse $(1, 0, 0)$ are spin-less. (c) right circular $(1, i, 0)$ and (d) left circular $(1, -i, 0)$ carry paraxial spins. (e) rolling forward $(1, 0, i)$ and (f) rolling backward $(1, 0, -i)$ carry non-paraxial spins. Here \mathbf{u} shows displacement trajectory. \mathbf{k} and \mathbf{s} represent wave vector and spin vector, respectively.

For stable propagation of rolling polarizations (Figs. 1(e) or 1(f)), the longitudinal and transverse components have to share the same phase velocity $c = \omega/k$. While this condition may be satisfied due to the effects of boundaries and interfaces, e.g., acoustic waves in air ducts [20], water waves in the ocean [34], Rayleigh waves along solid surfaces [35, 36] and Lamb waves in elastic plates [30], we can show that it is never satisfied for bulk waves in isotropic media.

Consider an isotropic elastic material with shear modulus μ , Poissons ratio ν , and mass density ρ : The ratio between the transverse phase velocity, c_T , and the longitudinal phase velocity, c_L , is given by

$$\frac{c_T}{c_L} = \sqrt{\frac{\mu}{\rho}} / \sqrt{\frac{2\mu(1-\nu)}{(1-2\nu)\rho}} = \sqrt{1 - \frac{1}{2(1-\nu)}}. \quad (5)$$

For static stability [37], we are constrained by $-1 \leq \nu \leq 1/2$ in 3D and $-1 \leq \nu \leq 1$ in 2D, both of which imply $c_T/c_L \leq \sqrt{3}/2$. Even if we disregard these constraints and allow for arbitrary values of the Poissons ratio, the speed ratio c_T/c_L can only asymptotically approach unity when $\nu \rightarrow \infty$. Therefore, as a frequency-independent material property, the *equal-speed criterion*, $c_T = c_L$, cannot be met by any isotropic medium.

As a consequence, we turn our attention to anisotropic media. For a plane wave with wave vector \mathbf{k} and wave number $k = |\mathbf{k}|$, we write

$$\tilde{\mathbf{k}} = \mathbf{k}/k = l_1 \mathbf{e}_1 + l_2 \mathbf{e}_2 + l_3 \mathbf{e}_3, \quad (6)$$

where l_1, l_2, l_3 are the direction cosines of the wave vector with respect to the Cartesian coordinate axes. We define a matrix \mathbf{L} as

$$\mathbf{L} = \begin{pmatrix} l_1 & 0 & 0 & 0 & l_3 & l_2 \\ 0 & l_2 & 0 & l_3 & 0 & l_1 \\ 0 & 0 & l_3 & l_2 & l_1 & 0 \end{pmatrix}, \quad (7)$$

and introduce the Kelvin-Christoffel matrix [38, 39]:

$$\mathbf{\Gamma} = \mathbf{L} \cdot \mathbf{C} \cdot \mathbf{L}^T \quad \text{or} \quad \Gamma_{ij} = L_{iI} C_{IJ} L_{jJ}, \quad (8)$$

where C_{IJ} is the elastic stiffness in Voigt notation ($I, J = 1, 2, 3 \dots 6$). Then, with the definition of phase velocity $c = \omega/k$, the wave equation can be written as [38, 39]:

$$\mathbf{\Gamma} \cdot \mathbf{u} - \rho c^2 \mathbf{u} = (\mathbf{\Gamma} - \rho c^2 \mathbf{I}) \cdot \mathbf{u} = \mathbf{0}. \quad (9)$$

Therefore, the *equal-speed criterion* is equivalent to the 3-by-3 matrix $\mathbf{\Gamma}$ having degenerate eigenvalues. For media with spatial symmetries, the criterion can be simplified further. Here we consider three examples for bulk waves propagating along the z -direction:

$$\text{2D } xz\text{-plane strain: } C_{33} = C_{55} \text{ and } C_{35} = 0 \quad (10a)$$

$$\text{Transversely } xy\text{-isotropic: } C_{33} = C_{44} \quad (10b)$$

$$\text{Cubic symmetric: } C_{11} = C_{44} \quad (10c)$$

To the best of our knowledge, the criteria listed in Eq. (10) are not satisfied by any existing materials, natural or synthetic. This motivates us to design metamaterials for this purpose. Aiming for structures that can be readily fabricated, we exclusively focus on architected geometries made from a single isotropic base material with Young's modulus E and Poisson's ratio $\nu = 0.3$. To identify suitable designs that work in the long wavelength limit, we perform quasi-static calculations using unit cells with appropriate periodic boundary conditions [40] on the finite element platform ABAQUS (element types CPE4 and C3D4). From the numerical results, we extract the dimensionless effective elastic constants $\bar{C}_{IJ} = C_{IJ}/E$.

First, we consider the 2D xz -plane strain case for waves propagating along the z -direction. In order to arrive at a micro-structure satisfying the equal-speed criterion, we need to strengthen the shear stiffness of the material without increasing its normal stiffness. Fig. 2(a) shows an example unit-cell, where the X-shaped center enhances the shear stiffness and the absence of vertical support reduces the normal stiffness. Using the numerical procedure described above, we calculate the dependence of the dimensionless effective elastic constants \bar{C}_{33} and \bar{C}_{55} on the geometry parameters L_1 and L_2 . The results are presented as two surfaces shown in Fig. 2(b). The equal-speed criterion is met at the line of intersection of the two surfaces. The geometry shown in Fig. 2(a) corresponds to the circled point at $(L_1/a, L_2/a) = (0.2, 0.1962)$. Next, as shown in Fig. 2(c), we present another 2D micro-structure satisfying Eq. (10a). This design was adapted from a previous study on dilatational materials [41], which in turn was based on earlier theoretical results [42]. The unit cell entails $C_{11} = C_{33}$ due to symmetry, and, hence, supports the propagation of rolling waves along both the x - and z -direction. The circled point $(b_1/a, b_2/a) = (0.01878, 0.005)$ in Fig. 2(d) corresponds to the geometry in Fig. 2(c) with $b_3 = b_4 = 0.05a$ and $b_5 = 0.3221a$. While this geometry was previously designed for auxetic (i.e., negative Poisson's ratio) properties [41], the parameters satisfying the equal-speed criterion actually result in a positive effective 2D Poisson's ratio between the principal directions, $\nu_{xz} = 0.996$. As this structure is strongly anisotropic, the fact that the principal Poisson's ratio approaches unity does not imply a large difference between c_T and c_L . We note that both 2D designs presented in Fig. 2 are mirror-symmetric with respect to both the x - and z -axis. This symmetry implies the absence of normal-to-shear or shear-to-normal couplings in the effective constitutive relations. Thus, irregardless of the geometry parameters, the condition $C_{35} = 0$ in Eq. (10a), holds for both structures."

In the 3D case, we consider highly symmetric geometries exhibiting either transverse isotropy or cubic symmetry. Fig. 3(a) shows the unit-cell design satisfying Eq. (10b). The honeycomb geometry is chosen to guarantee isotropy in the xy -plane. Each out-of-plane wall is constructed by

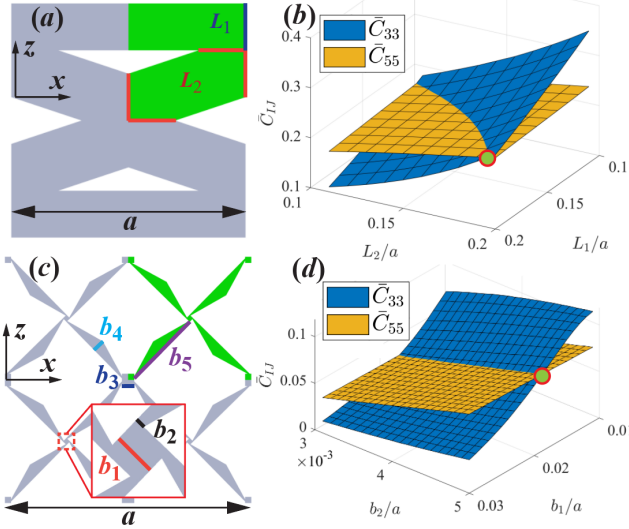


FIG. 2. 2D metamaterials capable of hosting rolling waves: (a) Unit cell design obtained by taking mirror images of the green quarter. Each red straight line segment is of length L_2 . (b) Numerically calculated effective elastic constants for the unit cell in (a) with varying geometric parameters. (c) Unit cell design adapted from [41]. It is obtained by taking mirror images of the green quarter. (d) Numerical results for the unit cell in (c) with $b_3 = b_4 = 0.05a$ and $b_5 = 0.3221a$. Geometries in (a) and (c) correspond to the circled points in (b) and (d), respectively.

extruding the planar pattern in Fig. 2(a). Besides L_1 and L_2 , the wall thickness, h , is an additional parameter of the 3D structure. Numerical results for the dimensionless constants, \bar{C}_{33} and \bar{C}_{44} are shown in Fig. 3(b) with $h/a = 0.2$ fixed. At the line of surface intersection, we obtain a set of designs satisfying the equal-speed criterion. The geometry in Fig. 3(a) corresponds to the circled point $(L_1/a, L_2/a) = (0.216, 0.1)$ in Fig. 3(b).

For the cubic symmetric case, a unit cell satisfying Eq. (10c) is shown in Fig. 3(c). This geometry was previously studied as an auxetic micro-structure [43]. It has the symmetry of the point group $m\bar{3}m$ - one of the cubic crystallographic point groups, which are characterized by four axes of three-fold rotational symmetry. The symmetry axes can be identified with the body diagonals of the cubic unit cell [41, 43, 44]. The cubic symmetry guarantees that the resulting stiffness matrix has a specific form with three independent elastic constants [39, 44, 45]. The unit cell in Fig. 3(c) is composed of identical beams with a square cross-section with side length L . For each of the six cubic faces, four beams extend from the vertices and meet at an interior point at a distance h_2 from the planar face center. By varying both L and h_2 , as shown in Fig. 3(d), we numerically find the line of intersection where the equal-speed criterion is satisfied. Parameters at the circled point $(L/a, h_2/a) = (0.06, 0.1035)$ correspond to the geometry in Fig. 3(c). While being auxetic in other directions, this structure actually has a positive

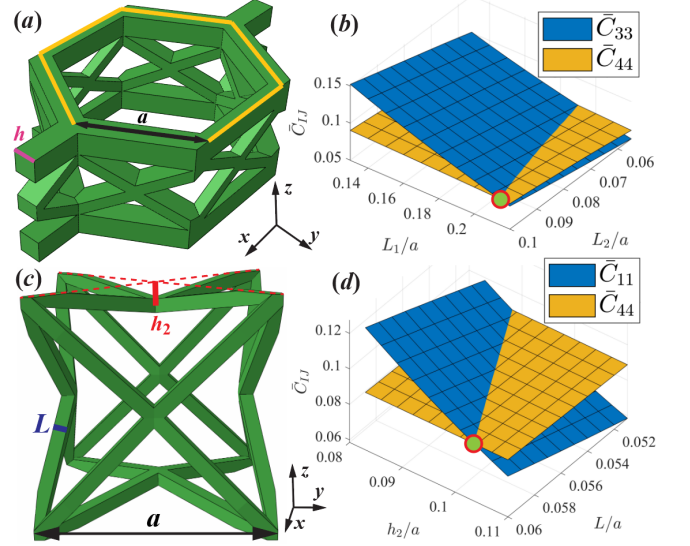


FIG. 3. 3D metamaterials capable of hosting rolling waves: (a) Honeycomb unit cell design based on the planar pattern shown in Fig. 2(a), exhibiting isotropy in the xy -plane. (b) Numerical results of effective elastic constants for the unit cell in (a) with $h = 0.2a$. (c) Unit cell design adapted from [43], exhibiting cubic symmetry. (d) Numerical results of the cubic case. Geometries in (a) and (c) correspond to the circled points in (b) and (d), respectively.

effective Poisson's ratio along its principal directions, as also shown in [43].

As an example of non-paraxial spin manipulation, we next investigate normal reflections of a rolling wave at a general elastic boundary. Considering a rolling wave along the z -direction normally incident on a flat surface, we have the instantaneous wave displacement fields at time $t = 0$ as $\mathbf{u}^I = \bar{\mathbf{u}}^I \exp(ikz)$ and $\mathbf{u}^R = \bar{\mathbf{u}}^R \exp(-ikz)$ with

$$\bar{\mathbf{u}}^I = \begin{pmatrix} m^I \\ n^I \\ l^I \end{pmatrix} \quad \text{and} \quad \bar{\mathbf{u}}^R = \begin{pmatrix} m^R \\ n^R \\ l^R \end{pmatrix}, \quad (11)$$

where the superscripts, I and R, denote the incident and reflected waves, respectively. For the surface at $z = 0$, we have

$$\sigma_{zj}^0 = K_j u_j^0, \quad j = x, y, z, \quad (12)$$

where K_j represents the distributed stiffness of a elastic foundation. At the surface, the stress σ_{zj}^0 and displacement u_j^0 are the superposition of the incident and reflected waves. By calculating the stresses and substituting them into the boundary conditions of (12), we obtain

$$m^R = R_x m^I, \quad n^R = R_y n^I, \quad l^R = R_z l^I, \quad (13)$$

with

$$R_j = \frac{C_{33}ik - K_j}{C_{33}ik + K_j}, \quad j = x, y, z. \quad (14)$$

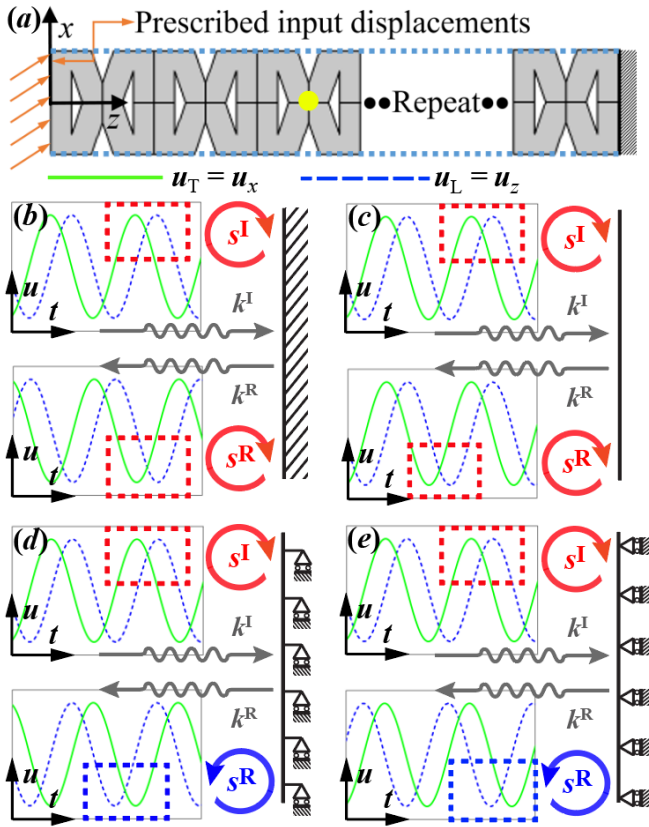


FIG. 4. Reflections of a rolling wave (with $s_y^I = -1$) for normal incidence: (a) Illustration of the setup for the time-domain numerical simulations. Periodic boundary conditions are applied on the top and bottom edges (dotted lines). A total number of 70 unit cells are used along the z -direction. Insets of (b)-(e) show the time history of displacements at the position marked by the yellow dot (•) in (a). (b) rigid and (c) free boundaries are both spin-preserving. (d) free-fixed and (e) fixed-free boundaries are both spin-flipping.

We next focus on 2D rolling waves in the xz -plane where the wave amplitudes in the y -direction vanish, $n^I = n^R = 0$. For $K_x = K_z = 0$, the boundary becomes traction-free (Neumann type) and we have $\tilde{\mathbf{u}}^R = \tilde{\mathbf{u}}^I$ with no phase change. For $K_x = K_z = \infty$, the boundary becomes rigid (Dirichlet type) and we have an out-of-phase reflected wave with $\tilde{\mathbf{u}}^R = -\tilde{\mathbf{u}}^I$. In both cases, we can obtain from Eq. (2) that $\mathbf{s}^R = \mathbf{s}^I$, so the spin is preserved. In contrast, for hybrid boundaries ($K_x = 0, K_z = \infty$) and ($K_x = \infty, K_z = 0$), similar analyses [39] result in $\mathbf{s}^R = -\mathbf{s}^I$, so the spin is flipped due to the difference in phase change between the longitudinal and transverse components during the reflection process. These behaviors are further demonstrated in time-domain simulations of a metamaterial made of unit cells shown in Fig. 2(a) using the commercial software COMSOL (quadratic quadrilateral elements). Fig. 4 shows the results for the incident rolling wave carrying a non-paraxial spin of $s_y^I = -1$. The reflection process is

spin-preserving in both rigid and free boundaries, while being spin-flipping for both hybrid free-fixed and hybrid fixed-free boundary conditions. Detailed numerical procedures and additional results of time-domain simulations are available in the Supplemental Material [39]. In summary, we studied elastic waves carrying non-paraxial spins, which can propagate in special anisotropic media satisfying the *equal-speed criterion*, $c_T = c_L$. We presented both 2D and 3D metamaterial designs satisfying this criterion. In addition, we analysed the reflection of such rolling waves incident on elastic boundaries, demonstrating spin-preserving and spin-flipping behaviors. In contrast to scattering-based [46–52] and resonance-based [53–60] metamaterials, our designs work in the non-resonant long-wavelength regime [61–65], essentially using exotic quasi-static properties for wave manipulations. All features shown in this study are *frequency independent* up to the cutoff threshold, which is only limited by how small we can make the unit cells. The tailored structures can be readily fabricated by existing techniques [66, 67]. This work lays a solid foundation for the new field of broadband phononic spin engineering.

This work was supported by start-up funds of the Dept. Mechanical Engineering at Univ. Utah. CK is supported by the NSF through Grant DMS-1814854. The authors thank Graeme Milton (Univ. Utah), Stephano Gonella (Univ. Minnesota), Liyuan Chen (Harvard Univ. & Westlake Univ.) and Bolei Deng (Harvard Univ.) for discussions. The support and resources from the Center for High Performance Computing at Univ. Utah are gratefully acknowledged.

-
- [1] Y. Long, J. Ren, and H. Chen, Proc. Natl. Acad. Sci. **115**, 9951 (2018).
 - [2] L. Burns, K. Y. Bliokh, F. Nori, and J. Dressel, New J. Phys. (2020).
 - [3] C. Shi, R. Zhao, Y. Long, S. Yang, Y. Wang, H. Chen, J. Ren, and X. Zhang, Natl. Sci. Rev. **6**, 707 (2019).
 - [4] P. Banzer, M. Neugebauer, A. Aiello, C. Marquardt, N. Lindlein, T. Bauer, and G. Leuchs, arXiv:1210.1772 (2012).
 - [5] J. Eismann, L. Nicholls, D. Roth, M. Alonso, P. Banzer, F. Rodríguez-Fortuño, A. Zayats, F. Nori, and K. Bliokh, arXiv:2004.02970 (2020).
 - [6] H. Zhu, J. Yi, M.-Y. Li, J. Xiao, L. Zhang, C.-W. Yang, R. A. Kaindl, L.-J. Li, Y. Wang, and X. Zhang, Science **359**, 579 (2018).
 - [7] J. Holanda, D. Maior, A. Azevedo, and S. Rezende, Nat. Phys. **14**, 500 (2018).
 - [8] X. Shi and J. Yang, arXiv:2004.02412.
 - [9] A. Rückriegel, S. Streib, G. E. Bauer, and R. A. Duine, Phys. Rev. B **101**, 104402 (2020).
 - [10] K. An, A. Litvinenko, R. Kohno, A. Fuad, V. Naleto, L. Vila, U. Ebels, G. de Loubens, H. Hurdequint, N. Beaulieu, *et al.*, Phys. Rev. B **101**, 060407 (2020).

- [11] B. Le Feber, N. Rotenberg, and L. Kuipers, *Nat. Commun.* **6**, 1 (2015).
- [12] I. Söllner, S. Mahmoodian, S. L. Hansen, L. Midolo, A. Javadi, G. Kiršanskė, T. Pregnolato, H. El-Ella, E. H. Lee, J. D. Song, *et al.*, *Nat. Nanotech.* **10**, 775 (2015).
- [13] L. Peng, L. Duan, K. Wang, F. Gao, L. Zhang, G. Wang, Y. Yang, H. Chen, and S. Zhang, *Nat. Photonics* **13**, 878 (2019).
- [14] K.-Y. Kim, I.-M. Lee, J. Kim, J. Jung, and B. Lee, *Phys. Rev. A* **86**, 063805 (2012).
- [15] S. Golat, E. A. Lim, and F. J. Rodríguez-Fortuño, *Phys. Rev. D* **101**, 084046 (2020).
- [16] S. Wang, G. Ma, and C. T. Chan, *Sci. Adv.* **4**, eaaq1475 (2018).
- [17] I. Toftul, K. Bliokh, M. Petrov, and F. Nori, *Phys. Rev. Lett.* **123**, 183901 (2019).
- [18] K. Y. Bliokh and F. Nori, *Phys. Rev. B* **99**, 174310 (2019).
- [19] K. Y. Bliokh and F. Nori, *Phys. Rev. B* **99**, 020301 (2019).
- [20] Y. Long, H. Ge, D. Zhang, X. Xu, J. Ren, M.-H. Lu, M. Bao, H. Chen, and Y.-F. Chen, *Natl. Sci. Rev.* (2020).
- [21] L. Calderin, M. A. Hasan, N. G. Jenkins, T. Lata, P. Lucas, K. Runge, and P. A. Deymier, *Sci. Rep.* **9**, 1 (2019).
- [22] S. Kumar, S. Tan, L. Zheng, and D. M. Kochmann, *NPJ Comput. Mater.* **6**, 1 (2020).
- [23] M. A. Hasan, L. Calderin, T. Lata, P. Lucas, K. Runge, and P. A. Deymier, *Appl. Phys. Lett.* **116**, 164104 (2020).
- [24] D. Liu and J. Shi, *Phys. Rev. Lett.* **119**, 075301 (2017).
- [25] W. Fu, Z. Shen, Y. Xu, C.-L. Zou, R. Cheng, X. Han, and H. X. Tang, *Nat. Commun.* **10**, 1 (2019).
- [26] Y. Liu, Y. Xu, W. Duan, *et al.*, *Research* **2019**, 5173580 (2019).
- [27] Y. Zhou, P. R. Bandaru, and D. F. Sievenpiper, *New J. Phys.* **20**, 123011 (2018).
- [28] S. Wu, Y. Wu, and J. Mei, *New J. Phys.* **20**, 023051 (2018).
- [29] M.-J. Tuo, L.-H. Zhang, D. Liu, R.-W. Peng, R.-H. Fan, Z.-G. Chen, Y. Wu, D.-X. Qi, and M. Wang, *Phys. Rev. B* **99**, 205432 (2019).
- [30] Y. Jin, W. Wang, Z. Wen, D. Torrent, and B. Djafari-Rouhani, *Extreme Mech. Lett.* , 100777 (2020).
- [31] D. Leykam, K. Y. Bliokh, and F. Nori, *arXiv:2004.04110* (2020).
- [32] L. Wei and F. J. Rodríguez-Fortuño, *arXiv:2003.13292* (2020).
- [33] M. V. Berry, *J. Opt. A* **11**, 094001 (2009).
- [34] C. Li, L. Xu, L. Zhu, S. Zou, Q. H. Liu, Z. Wang, and H. Chen, *Phys. Rev. Lett.* **121**, 104501 (2018).
- [35] S. Brule, S. Enoch, and S. Guenneau, *arXiv:2004.07037* (2020).
- [36] Y. Zhao, X. Zhou, and G. Huang, *J. Mech. Phys. Solids* , 104065 (2020).
- [37] L. Landau and E. Lifshitz, Chapter iii - Elastic waves, in *Theory of Elasticity* (Pergamon Press, 1970) second edition ed., p. 102.
- [38] J. M. Carcione, *Wave fields in real media: Wave propagation in anisotropic, anelastic, porous and electromagnetic media* (Elsevier, 2007).
- [39] For more details, see Supplemental Material at [URL], which includes References [37, 38, 41, 68–72].
- [40] J. T. Overvelde and K. Bertoldi, *J. Mech. Phys. Solids* **64**, 351 (2014).
- [41] T. Bückmann, R. Schittny, M. Thiel, M. Kadic, G. W. Milton, and M. Wegener, *New J. Phys.* **16**, 033032 (2014).
- [42] G. W. Milton, *J. Mech. Phys. Solids* **61**, 1543 (2013).
- [43] J. Dirrenberger, S. Forest, and D. Jeulin, *Int. J. Mech. Mater. Des.* **9**, 21 (2013).
- [44] A. Authier, *International tables for crystallography: Volume D: Physical properties of crystals* (Wiley Online Library, 2003).
- [45] A. N. Norris, *Proc. Roy. Soc. A* **462**, 3385 (2006).
- [46] H. He, C. Qiu, L. Ye, X. Cai, X. Fan, M. Ke, F. Zhang, and Z. Liu, *Nature* **560**, 61 (2018).
- [47] B. Deng, P. Wang, Q. He, V. Tournat, and K. Bertoldi, *Nat. Commun.* **9**, 1 (2018).
- [48] P. Celli, B. Yousefzadeh, C. Daraio, and S. Gonella, *Appl. Phys. Lett.* **114**, 091903 (2019).
- [49] Y.-F. Wang, J.-W. Liang, A.-L. Chen, Y.-S. Wang, and V. Laude, *Phys. Rev. B* **101**, 184301 (2020).
- [50] Y. Xia, E. Riva, M. I. Rosa, G. Cazzulani, A. Erturl, F. Braghin, and M. Ruzzene, *arXiv:2006.07348* (2020).
- [51] M. Rosa, M. Ruzzene, and E. Prodan, *arXiv:2006.10019* (2020).
- [52] V. Ramakrishnan and M. Frazier, *J. Appl. Mech.* **127**, 225104 (2020).
- [53] A. Palermo, Y. Wang, P. Celli, and C. Daraio, *Phys. Rev. Appl.* **11**, 044057 (2019).
- [54] I. Arretche and K. H. Matlack, *J. Appl. Mech.* **86** (2019).
- [55] W. Wang, Y. Jin, W. Wang, B. Bonello, B. Djafari-Rouhani, and R. Fleury, *Phys. Rev. B* **101**, 024101 (2020).
- [56] C. Sugino, M. Ruzzene, and A. Erturk, *Phys. Rev. Appl.* **13**, 061001 (2020).
- [57] M. I. Hussein, C.-N. Tsai, and H. Honarvar, *Adv. Funct. Mater.* **30**, 1906718 (2020).
- [58] M. A. Ghanem, A. Khanolkar, H. Zhao, and N. Boechler, *Adv. Funct. Mater.* **30**, 1909217 (2020).
- [59] H. Nassar, Y. Chen, and G. Huang, *Phys. Rev. Lett.* **124**, 084301 (2020).
- [60] O. R. Bilal, A. Foehr, and C. Daraio, *J. Appl. Mech.* **87** (2020).
- [61] M. Zheng, X. Liu, Y. Chen, H. Miao, R. Zhu, and G. Hu, *Phys. Rev. Appl.* **12**, 014027 (2019).
- [62] G. U. Patil, A. B. Shedge, and K. H. Matlack, *Appl. Phys. Lett.* **115**, 091902 (2019).
- [63] R. Behrou, M. A. Ghanem, B. C. Macnider, V. Verma, R. Alvey, J. Hong, A. F. Emery, H. A. Kim, and N. Boechler, *arXiv:2005.09111* (2020).
- [64] M. Zheng, C. I. Park, X. Liu, R. Zhu, G. Hu, and Y. Y. Kim, *Appl. Phys. Lett.* **116**, 171903 (2020).
- [65] X. Xu, C. Wang, W. Shou, Z. Du, Y. Chen, B. Li, W. Matusik, N. Hussein, and G. Huang, *Phys. Rev. Lett.* **124**, 114301 (2020).
- [66] W. Liu, H. Song, and C. Huang, *Addit. Manuf.* , 101257 (2020).
- [67] B. Elder, R. Neupane, E. Tokita, U. Ghosh, S. Hales, and Y. L. Kong, *Adv. Mater.* **32**, 1907142 (2020).
- [68] P. Wang, F. Casadei, S. H. Kang, and K. Bertoldi, *Phys. Rev. B* **91**, 020103 (2015).
- [69] P. Zhang, P. Wei, and Y. Li, *Meccanica* **52**, 1641 (2017).
- [70] Y. Chen, M. Kadic, S. Guenneau, and M. Wegener, *Phys. Rev. Lett.* **124**, 235502 (2020).
- [71] Y. Ding, Z. Liu, C. Qiu, and J. Shi, *Phys. Rev. Lett.* **99**, 093904 (2007).
- [72] A. S. Phani, J. Woodhouse, and N. Fleck, *J. Acoust. Soc. Am.* **119**, 1995 (2006).